ELSEVIER

Mathematics and Computers in Simulation 61 (2003) 497–507

MATHEMATICS AND COMPUTERS IN SIMULATION

www.elsevier.com/locate/matcom

Numerical analysis of dynamic characteristics of coupled piezoelectric systems in acoustic media

Roderick V.N. Melnik*

Mads Clausen Institute, University of Southern Denmark, Grundvigs Alle 150, DK-6400 Sonderborg, Denmark

Abstract

In this paper, the full dynamic model describing vibrations of piezoceramic solids of hollow cylindrical shapes and accounting for the coupling of the solids to surrounding fluid/gas media has been analysed numerically. The major attention has been given to the case of radial preliminary polarisation of piezoceramics where a strong coupling between electric and mechanical fields is an essential feature of the dynamics. An efficient numerical discretisation scheme based on the integro-interpolation approach has been proposed and representative examples of computational experiments are given.

MSC: 35M10; 74F20; 65M06

Keywords: Piezoelectrics; Acoustic media; Dynamics; Integro-interpolational schemes

1. Introduction

Waves propagation in anisotropic media has always been a topic of immense practical importance and a rich source of new challenges for applied mathematicians [1,6–8,10,12,15,18,21]. Purely elastic waves in shells have been studied intensively in the context of fluid-structure interactions at least since late 1950s and new practical applications have continued to fuel interest to such studies (e.g. [1,8] and references therein). However, when it comes to the study of *coupled*, such as electromechanical, waves in *anisotropic* hollow shells surrounded in addition by acoustic media, both internally and externally, the situation becomes much more involved and little is know about the general *dynamic* case. It is these types of problems that are of interest in the present paper. For such problems, where general time-dependent (not necessarily harmonic) patterns of coupled electromechanical loadings can be applied to the piezoelectric element the analytical technique has a limited applicability, unless quite restrictive assumptions, in particular on the electromechanical loadings and/or electric fields patterns are imposed [10,20]. The full dynamic treatment of such problems based on effective numerical techniques is required.

* Tel.: +45-6550-1681; fax: +45-6550-1660.
E-mail address: rmelnik@mci.sdu.dk (R.V.N. Melnik).

0378-4754/02/$ – see front matter
PII: S0378-4754(02)00100-3

There are two major distinctive features of this paper. First, it focuses on the case of radial preliminary polarisation of the piezoceramic where, in contrast to the axial and circular preliminary polarisation cases, the coupling between electric and mechanical fields is very strong [14,15]. Secondly, this paper is a contribution to the study of the full dynamic behaviour of piezoelectric solids (and therefore goes beyond often considered cases of harmonic patterns of loadings and travelling wave solutions [4,20,21]), accounting at the same time for the coupling with the surrounding (internal and external) media.

In terms of topological designs, our main attention is devoted to hollow cylinders because they have been and they continue to be ones of the most important constructive elements in civil engineering and aerospace, especially when are used as industrial pipes, as well as for muffler acoustics, wind musical instruments, aeronautical shells, etc. [7]. In many applications, these constructive elements are essentially anisotropic as it is the case with piezoceramic shells widely used in transducer applications, ultrasonic SAW devices and flow-meters, biomedical engineering applications and smart materials and structures technology [5,6,14,15]. Such advanced applications of hollow piezoceramic elements require using models that account for an intrinsic *dynamic coupling* between three media that might have distinctively different acoustic properties, that is the piezoelectric medium and two other media surrounding internal and external surfaces of the element.

In this paper, we construct our model by coupling three hyperbolic-type equations (the equation of motion for piezoelectric media and two equations for pressure fields of the surrounding media) with an elliptic equation (Maxwell's equation for dielectrics). The problem is supplemented by appropriate initial and boundary conditions and solved numerically with an efficient numerical scheme derived from the integro-interpolational methodology. Finally, a representative example of numerical experiments for a PZT piezoceramics is given.

2. Dynamic models for coupled electromechanical systems

Consider the following general model describing coupled electromechanical motion of piezoelectric solids (e.g. [9,15])

$$\rho\frac{\partial^2 \boldsymbol{u}}{\partial t^2} = \nabla\cdot\boldsymbol{\sigma} + \boldsymbol{F}, \qquad \mathrm{div}\boldsymbol{D} = \boldsymbol{G}, \qquad \boldsymbol{E} = -\nabla\varphi, \tag{2.1}$$

written here in the Cartesian system of coordinates $\boldsymbol{x} = (x_1, x_2, x_3)^{\mathrm{T}}$. In (2.1), $\boldsymbol{u} = (u_1, u_2, u_3)^{\mathrm{T}}$ is the displacement vector, ρ the density of piezoelectric material, $\boldsymbol{G}$ and $\boldsymbol{F}$ the electric and body forces on the piezoelectric (if any), φ the electrostatic potential. The actual form of the constitutive equations for this model depends on the choice of the thermodynamic potential, which is chosen here in the form of electric enthalpy $H(\boldsymbol{\epsilon}_v, \boldsymbol{E})$. In this case, the symmetric stress tensor (represented here as $\boldsymbol{\sigma}_v = (\sigma_x, \sigma_y, \sigma_z, \sigma_{yz}, \sigma_{xz}, \sigma_{xy})^{\mathrm{T}}$) is coupled to the electric field strength ($\boldsymbol{E}$), and the electric induction $\boldsymbol{D}$ is coupled to the mechanical field strains (represented due to symmetry as $\boldsymbol{\epsilon}_v = (\epsilon_x, \epsilon_y, \epsilon_z, \epsilon_{yz}, \epsilon_{xz}, \epsilon_{xy})^T$) by the following relations

$$\boldsymbol{\sigma}_v = \boldsymbol{c}\boldsymbol{\epsilon}_v - \boldsymbol{e}^{\mathrm{T}}\boldsymbol{E}, \qquad \boldsymbol{D} = \boldsymbol{\varepsilon}\boldsymbol{E} + \boldsymbol{e}\boldsymbol{\epsilon}_v, \tag{2.2}$$

where $\boldsymbol{c} = (c_{ij})$, $i, j = 1, \ldots, 6$ are elastic coefficients, $\boldsymbol{e} = (e_{ij})$, $i = 1, 2, 3$, $j = 1, \ldots, 6$ are piezomoduli, and $\boldsymbol{\varepsilon} = (\varepsilon_{ij})$, $i, j = 1, 2, 3$ are dielectric permittivities. The strain tensor is related to the displacements by the standard Cauchy relation which in the tensorial form is written as $2\boldsymbol{\epsilon}_{ij} = u_{i,j} + u_{j,i}$, where

$\boldsymbol{\epsilon}_{ij}$, $i = 1, 2, 3$ is the full (symmetric) strain matrix with element components given in $\boldsymbol{\epsilon}_v$. In such a general formulation, even without accounting for acoustic pressures of the surrounding media, one has to deal (assuming a triclinic crystal structure [9,17]) with 45 material constants, that is 21 elastic, 18 piezoelectric and six dielectric coefficients. Fortunately, the general model (2.1) and (2.2) can be simplified in the case of piezoceramics because these materials behave themselves like transversely-isotropic bodies for which the symmetry axis coincides with the direction of the preliminary polarisation. This reduces our consideration to just 10 material electromechanical constants (five elastic, three piezomodules, and two dielectric coefficients). In the terminology of crystallographic point groups [9], this corresponds to a specific subsystem of hexagonal systems which has a six-fold rotation axis or inversion. In what follows this subsystem (which belongs to the class 6 mm and has a six-fold symmetry axis parallel to $0Z$) is in the focus of our attention. Note however that the numerical methodology developed in this paper can be adapted to other classes of symmetry, e.g. to a lower symmetry orthorhombic systems of class mm2 (e.g. [9,17]).

3. Basic microstructural models of piezoelectric materials, preliminary polarisation, and topological design

Natural piezoelectric crystals are not easily amenable to geometrical shapes that are important in many applications. This fact leads to a situation where artificial piezoelectrics, and in particular piezoceramics, have become the main materials in a vast majority of industrial applications of piezoelectrics. Piezoelectric ceramics can be thought as a polycrystallic solid containing elementary dipoles, as a consequence of non-symmetry of the crystallic lattice (crystals with a center of symmetry do not exhibit piezoelectric effect). In brief, dipoles tend to be oriented stochastically with respect to each other, but at a smaller scale they tend to be parallel to each other in small regions known as domains. If an external electric field is applied to the domain a change of its size is induced indicating the piezoelectric properties of the domain. This effect is not pronounced at the macroscopic level without special prior treatment of piezoceramics, and a strong electric field (e.g. 25–35 kV/cm) should be applied in order to arrange the domain in one single direction.

It is important to emphasise that the type of preliminary polarisation determines the actual form of constitutive Eq. (2.2), and therefore the pattern of coupling between electric and mechanical fields. With few exceptions [3,12,15] (see also references therein), most studies performed so far in the literature for the dynamic case concern with the axial preliminary polarisation in which case constitutive equations for circular cylinders coincide with the state equations for piezoelectric *crystals* of class 6 mm with the symmetry axis OZ, and therefore follow in a trivial manner from (2.2) by setting $\boldsymbol{\sigma}_v = (\sigma_r, \sigma_\theta, \sigma_z, \sigma_{\theta z}, \sigma_{rz}, \sigma_{r\theta})^{\mathrm{T}}$, $\boldsymbol{\epsilon}_v = (\epsilon_r, \epsilon_\theta, \epsilon_z, 2\epsilon_{\theta z}, 2\epsilon_{rz}, 2\epsilon_{r\theta})^{\mathrm{T}}$, $\boldsymbol{E} = (E_r, E_\theta, E_z)^{\mathrm{T}}$, and $\boldsymbol{D} = (D_r, D_\theta, D_z)^{\mathrm{T}}$. In the general case, however, the direction of the external field is not necessarily homogeneous and may change inside the volume of the solid, and therefore strictly speaking coefficients in the above constitutive equations should be coordinate-dependent. Only in the case where the external field of preliminary polarisation has some symmetry properties, it is possible to derive constitutive equations with constant coefficients in appropriate curvilinear systems of coordinates, and the most practical types of preliminary polarisation for cylindrical shells are axial, radial, and circular (e.g. [4,14] and references therein). We focus here on the case of radial preliminary polarisation where the material exhibits a substantially different pattern of coupling compared to better studied cases of axial and circular preliminary polarisations. In particular,

we have (e.g. [3,4,15] and references therein)

$$\boldsymbol{c} = \begin{pmatrix} c_{33} & c_{13} & c_{13} & 0 & 0 & 0 \\ c_{13} & c_{11} & c_{12} & 0 & 0 & 0 \\ c_{13} & c_{12} & c_{11} & 0 & 0 & 0 \\ 0 & 0 & 0 & c_{55} & 0 & 0 \\ 0 & 0 & 0 & 0 & c_{66} & 0 \\ 0 & 0 & 0 & 0 & 0 & c_{55} \end{pmatrix}, \qquad c_{66} = \tfrac{1}{2}(c_{11} - c_{12}), \tag{3.1}$$

$$\boldsymbol{\varepsilon} = \begin{pmatrix} \varepsilon_{33} & 0 & 0 \\ 0 & \varepsilon_{11} & 0 \\ 0 & 0 & \varepsilon_{11} \end{pmatrix}, \qquad \boldsymbol{e} = \begin{pmatrix} e_{33} & e_{31} & e_{31} & 0 & 0 & 0 \\ 0 & 0 & 0 & e_{15} & 0 & 0 \\ 0 & 0 & 0 & 0 & e_{15} & 0 \end{pmatrix}. \tag{3.2}$$

Note that it is easy to confirm that constitutive Eqs. (2.2), (3.1) and (3.2) have the form intrinsic to the class 6 mm if we introduce the following new vectors $\boldsymbol{\sigma}^r_{6\,\mathrm{mm}} = (\sigma_\theta, \sigma_z, \sigma_r, \sigma_{rz}, \sigma_{r\theta}, \sigma_{\theta z})^{\mathrm{T}}$, $\boldsymbol{\epsilon}^r_{6\,\mathrm{mm}} = (\epsilon_\theta, \epsilon_z, \epsilon_r, 2\epsilon_{rz}, 2\epsilon_{r\theta}, 2\epsilon_{\theta z})^{\mathrm{T}}$, $\boldsymbol{E}^r_{6\,\mathrm{mm}} = (E_\theta, E_z, E_r)^{\mathrm{T}}$, and $\boldsymbol{D}^r_{6\,\mathrm{mm}} = (D_\theta, D_z, D_r)^{\mathrm{T}}$. Moreover, in order to relate all three types of preliminary polarisations mentioned here to the same class of piezoceramic (class 6 mm) the following ordering of axes should be used (Cartesian to cylindrical) (a) $(x_1, x_2, x_3) \to (r, \theta, z)$ in the case of axial preliminary polarisation, (b) $(x_1, x_2, x_3) \to (\theta, z, r)$ in the case of the radial preliminary polarisation, (c) $(x_1, x_2, x_3) \to (z, r, \theta)$ in the case of circular preliminary polarisation (e.g. [4]). The general models (2.1), (2.2), (3.1) and (3.2) consisting of 22 equations with 22 unknowns (three components of displacements, the electric field strength, electric field induction vectors, six components of stress and strain tensors, and the electrostatic potential) is the basis for our further consideration.

4. Dynamic behaviour of hollow piezoceramic cylinders under different types of preliminary polarisation

We are interested in axisymmetric dynamic behaviour of piezoceramic shells, and therefore the systems (2.1) and (2.2) can be simplified to

$$\rho \begin{pmatrix} \dfrac{\partial^2 u_r}{\partial t^2} \\ \dfrac{\partial^2 u_z}{\partial t^2} \end{pmatrix} = \frac{\partial}{\partial r}\begin{pmatrix} \sigma_r \\ \sigma_{rz} \end{pmatrix} + \frac{\partial}{\partial z}\begin{pmatrix} \sigma_{rz} \\ \sigma_z \end{pmatrix} + \frac{1}{r}\begin{pmatrix} \sigma_r - \sigma_\theta \\ \sigma_{rz} \end{pmatrix} + \boldsymbol{F}, \tag{4.1}$$

$$\frac{1}{r}\frac{\partial}{\partial r}(rD_r) + \frac{\partial D_z}{\partial z} = 0. \tag{4.2}$$

The Cauchy relationships in this case have the form

$$\epsilon_r = \frac{\partial u_r}{\partial r}, \qquad \epsilon_\theta = \frac{u_r}{r}, \qquad \epsilon_z = \frac{\partial u_z}{\partial z}, \qquad 2\epsilon_{rz} = \frac{\partial u_r}{\partial z} + \frac{\partial u_z}{\partial r},$$
$$E_r = -\frac{\partial \varphi}{\partial r}, \qquad E_z = -\frac{\partial \varphi}{\partial z}. \tag{4.3}$$

As before, constitutive equations can be represented in the form (2.2). However, the dimensionality of vectors and matrices in those expressions are now reduced. We introduced the following vectors

$$\boldsymbol{\sigma}_v = (\sigma_r, \sigma_\theta, \sigma_z, \sigma_{rz})^{\mathrm{T}}, \qquad \boldsymbol{\epsilon}_v = (\epsilon_r, \epsilon_\theta, \epsilon_z, 2\epsilon_{rz})^{\mathrm{T}}, \qquad \boldsymbol{E} = (E_r, E_z)^{\mathrm{T}},$$
$$\boldsymbol{D} = (D_r, D_z)^{\mathrm{T}}, \tag{4.4}$$

and for the brevity reason, we give the data for the case of radial polarisation only, the case for which computational experiments were performed (simplified matrices consisting only of columns and rows relevant to this axisymmetric case are given):

$$\boldsymbol{c} = \begin{pmatrix} c_{33} & c_{13} & c_{13} & 0 \\ c_{13} & c_{11} & c_{12} & 0 \\ c_{13} & c_{12} & c_{22} & 0 \\ 0 & 0 & 0 & c_{55} \end{pmatrix}, \qquad \varepsilon = \begin{pmatrix} \varepsilon_{33} & 0 \\ 0 & \varepsilon_{11} \end{pmatrix}, \qquad \boldsymbol{e} = \begin{pmatrix} e_{33} & e_{31} & e_{31} & 0 \\ 0 & 0 & 0 & e_{15} \end{pmatrix}. \tag{4.5}$$

5. Mathematical models for acoustic media surrounding piezoelectric systems

The interior and/or exterior of the piezoceramic cylindrical shell used in applications can be surrounded by acoustic (fluid/gas) media. The coupling of the shell to such media is modelled here via the acoustic pressure, coupled in its turn to the flow velocity. Hence, in addition to (4.1)–(4.5) in the case of axisymmetric waves, we have two pairs of 3 equations (the continuity equation coupled with two equations resulted from Euler's vector equation with respect to components of the fluid particle velocity $\boldsymbol{v}^{(i)} = (v_r^{(i)}, v_z^{(i)})$, $i = 1, 2$) on each side of the hollow piezoceramic shell

$$\frac{1}{\rho_i c_i^2}\frac{\partial p_i}{\partial t} + \frac{1}{r}\left(r\frac{\partial v_r^{(i)}}{\partial r}\right) + \frac{\partial v_z^{(i)}}{\partial z} = 0, \qquad \rho_i \frac{\partial v_r^{(i)}}{\partial t} + \frac{\partial p_i}{\partial r} = 0, \qquad \rho_i \frac{\partial v_z^{(i)}}{\partial t} + \frac{\partial p_i}{\partial z} = 0, \tag{5.1}$$

where ρ_i, c_i, and p_i $(i = 1, 2)$ denote densities, speeds of sound, and acoustic pressures in the internal and external media, surrounding the piezoelectric body. These equations are coupled with the electromechanical system by means of the matching boundary conditions. In particular, the mechanical boundary conditions for the cylinder interior ($r = R_1$) and exterior ($r = R_2$) include the condition for pressure continuity on the radial boundary of the shell

$$\sigma_r(R_1 + 0, z, t) = -P_1(R_1 - 0, z, t), \qquad \sigma_r(R_2 - 0, z, t) = -P_2(R_2 + 0, z, t), \tag{5.2}$$

where $P_i(R_i + 0, z, t) = -\rho_i \partial\varphi_i/\partial t$; $i = 1, 2$ are acoustic pressures of the flows on the internal and external surfaces of the piezoceramic cylinder, respectively, and φ_i, $i = 1, 2$ are velocity potentials ($\boldsymbol{v}^{(i)} = \nabla\varphi_i$) in the corresponding region. Note that the last relationship is obtained by the same arguments from the Navier–Stokes equation as, for example, in [8,11]. Based on such arguments, it is also easy to obtain modified wave equations for the acoustic pressures p_i

$$\left(1 + \tau_i \frac{\partial}{\partial t}\right)\nabla^2 p_i = \frac{1}{c_i^2}\frac{\partial^2 p_i}{\partial t^2}, \quad i = 1, 2 \tag{5.3}$$

with τ_i being a relaxation time responsible for a combined mechanism of energy losses in the corresponding medium (due to viscosity, etc.). Then, following [11] (pp. 146–147), it can be shown that for the

case of irrotational fields, we have $(1+\tau_i\partial/\partial t)p = -\rho_i\partial\varphi_i/\partial t$. Hence, if $\tau_i = 0$ (as is assumed on the solid/fluid or solid/gas boundary interface), we obtain a relation coupling the pressure in the fluid/gas and the velocity potential $p_i = -\rho_i\partial\varphi_i/\partial t$, which is used frequently in applications (e.g. [18]). This relation is used for the boundary conditions (5.2). The complete set of mechanical boundary conditions can be found in [15]. Our numerical procedure is demonstrated in the next section for the so-called infinitely long piezoceramic cylinders, in which case only the conditions (5.2) are necessary. The specification of electrical boundary conditions depend on the presence and location of "internal" electrodes. We assume here that the cylinder is exited by an electric pulse with the pre-defined (possibly time-varying) applied potential difference $2V(t)$, and therefore, we have

$$\varphi = V(t), \qquad r = R_1; \qquad \varphi = -V(t), \qquad r = R_2 \tag{5.4}$$

(other electrical conditions, see e.g. [15,20], can be also implemented). Finally, the continuity of the radial components of the velocity on the both internal and external surfaces of the piezoelectric cylindrical shell is assumed (recall that the flow is irrotational, and hence $v_r(R_1-0,z,t) = \partial\varphi_1/\partial r$ and $v_r(R_2+0,z,t) = \partial\varphi_2/\partial r$):

$$\frac{\partial u_r}{\partial t}(R_1+0,z,t) = \frac{\partial\varphi_1}{\partial r}, \qquad \frac{\partial u_r}{\partial t}(R_2-0,z,t) = \frac{\partial\varphi_2}{\partial r}. \tag{5.5}$$

6. Discrete models with exemplification given for infinitely long piezoelectric cylinders surrounded by acoustic media

We explain the basic ideas of our numerical approximation based on the assumption that the longitudinal length of the cylinder exceeds substantially its thickness. In this case, the problem is considered in the spatial-temporal region $Q_T = G\times[0,T]$ with $G = [R_0, R_3]$, where $R_0 \le R_1 < R_2 < R_3$. In particular, we have the equation of motion and the Maxwell equation (e.g. [12])

$$\rho_0\frac{\partial^2 u}{\partial t^2} = \frac{1}{r}\frac{\partial}{\partial r}(r\sigma_r) - \frac{\sigma_\theta}{r} + F(r,t), \qquad \frac{1}{r}\frac{\partial}{\partial r}(rD_r) = G(r,t), \qquad (r,t)\in(R_1,R_2)\times[0,T], \tag{6.1}$$

coupled by the constitutive equations resulted from the radial preliminary polarisation

$$\sigma_r = c_{33}\epsilon_r + c_{13}\epsilon_\theta - e_{33}E_r, \quad \sigma_\theta = c_{13}\epsilon_r + c_{11}\epsilon_\theta - e_{31}E_r, \quad D_r = \varepsilon_{33}E_r + e_{31}\epsilon_\theta + e_{33}\epsilon_r. \tag{6.2}$$

Note that for mathematical convenience tensorial notations of the coefficients in (6.2) are sometimes chosen in a different way, but here we keep the notation of the general case considered in the previous sections. Instead of (5.3) considered for $\tau_i = 0$, we use here equivalent equations written in terms of the flow velocity potentials φ_1 and φ_2 in the cylindrical coordinates

$$\frac{\partial^2\varphi_i}{\partial t^2} - c_i^2\frac{1}{r}\frac{\partial}{\partial r}\left(r\frac{\partial\varphi_i}{\partial r}\right) = 0, \quad i = 1,2. \tag{6.3}$$

Eqs. (6.1)–(6.3) are coupled by the electromechanical boundary conditions. In particular, as before, we require the continuity conditions for pressures and velocities, which in the case considered in this section

have the form

$$\sigma_r = -P_i(t), \quad \frac{\partial u}{\partial t} = \frac{\partial \varphi_i}{\partial r} \quad \text{with} \quad i = 1 \quad \text{for} \quad R = R_1, \quad \text{and} \quad i = 2 \quad \text{for} \quad R = R_2. \tag{6.4}$$

The electrical boundary conditions are identical to (5.4). Initial conditions follow naturally from our consideration by assuming that displacements, their velocities, as well as acoustic potentials, and their time derivatives are zeros in the unperturbed state

$$u = 0, \quad \frac{\partial u}{\partial t} = 0, \qquad \varphi_j = \frac{\partial \varphi_j}{\partial t} = 0, \quad j = 1, 2, \quad t = 0. \tag{6.5}$$

Finally, we impose the following limiting conditions on the behavior of the surrounding flows

$$\lim_{r\to 0} \varphi_1 < \infty, \quad \lim_{r\to\infty} \varphi_2 = 0. \tag{6.6}$$

The condition of boundedness of potential φ_1 is replaced by $\lim_{r\to 0} r\,\partial\varphi_1/\partial r = 0$ (see, e.g. [2,19]), and for computational purposes, we replace the second condition in (6.6) by $\lim_{r\to R_3}\varphi_2 = 0$ with R_3 being sufficiently large.

Now we are in a position to underline the basic steps of the proposed discretisation procedure with a special attention given to the approximations of matching boundary conditions between fluid and solid parts of the system. This problem has been addressed in part in [2,5,12,13], but no general approaches for the strongly coupled (with radial preliminary polarisation) case in the full dynamic situation have been proposed. Some related results on well-posedness, a priori estimates, stability conditions, and accuracy in classes of generalised solutions can be found in [12,13,15]. We introduce standard computational grid $\bar\omega = \bar\omega_\tau \times \prod_{i=1}^3 \bar\omega_i$ in $Q_T = [R_0, R_3] \times [0, T]$ (e.g. [19]), where $\bar\omega_1$ and $\bar\omega_3$ are spatial computational grids for inside and outside flows surrounding the solid, and $\bar\omega_2$ is the spatial computational grid for the piezoelectric body itself (see Fig. 1). For example, we can use the following locally uniform grids $\bar\omega_k = \{r_i^{(k)} = R_{k-1} + ih_k; i = 0, 1, \ldots, N_k; h_k = (R_k - R_{k-1})/N_k\}, k = 1, 2, 3$, and $\bar\omega_\tau = \{t^n = n\tau, n = 0, 1, \ldots, K\}$, where $K\tau = T$, $r_{N_1}^{(1)} = r_0^{(2)}$, and $r_{N_2}^{(1)} = r_0^{(3)}$. The discrete analogues of the quadruple of the unknown functions $(\varphi_1, u, \varphi, \varphi_2)$ are denoted by (v, y, μ, w), respectively. Hence, function v is defined on $\bar\omega_\tau \times \bar\omega_1$ and coupled to function y defined on $\bar\omega_\tau \times \bar\omega_2$ by matching conditions at $r_{N_1}^{(1)} = r_0^{(2)}$. Functions y and μ are coupled on $\bar\omega_\tau \times \bar\omega_2$. In addition, function y is coupled to function w defined on $\bar\omega_\tau \times \bar\omega_3$ by matching conditions at $r_{N_2}^{(1)} = r_0^{(3)}$. Discretisation of the models (6.1)–(6.6) in $\tilde Q_T = (R_1, R_2) \times I$ with $I = [0, T]$ can be obtained first by using the variational approach based on the definition of the generalised solution pair $(u, \varphi) \in W_2^1(\tilde Q_T) \times L_2(I, W_2^1(R_1, R_2))$ [12,13], and then by deriving the energy balance identity and its discrete analogue. Following the two-step procedure described in detail in [12,13],

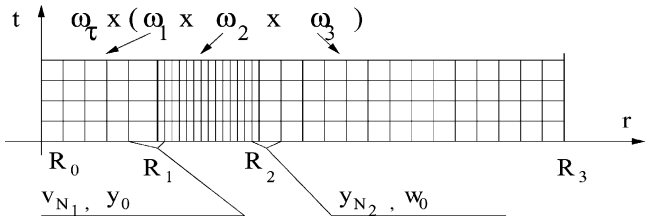

Fig. 1. A schematic grid generation.

we obtain discrete approximations of the equations describing the dynamics of the piezoelectric solid

$$\rho_2 \frac{\Delta y^n}{\tau^2} = \frac{1}{r}\frac{(\bar{r}\bar{\sigma}_r)^{(+1)} - \bar{r}\bar{\sigma}_r}{h_2} - \frac{(\bar{\sigma}_\theta)^{(+1)} + \bar{\sigma}_\theta}{2r} + F, \qquad \frac{1}{r}\frac{(\bar{r}\bar{D}_r)^{(+1)} - \bar{r}\bar{D}_r}{h_2} = G, \tag{6.7}$$

where the state equations are approximated in the "flux" grid points with $\bar{\epsilon}_r = (y - y^{(-1)})/h_2$, $\bar{\epsilon}_\theta = (y + y^{(-1)})/2\bar{r}$, $\Delta y^n = y^{n+1} - 2y^n + y^{n-1}$, super-indices "±" indicate the right/left shift for one grid point in the spatial direction, $\bar{E}_r = -(\mu - \mu^{(-1)})/h_2$ and

$$\begin{aligned} &\bar{\sigma}_r = c_{33}\bar{\epsilon}_r + c_{13}\bar{\epsilon}_\theta - e_{33}\bar{E}_r, \qquad \bar{\sigma}_\theta = c_{13}\bar{\epsilon}_r + c_{11}\bar{\epsilon}_\theta - e_{31}\bar{E}_r, \\ &\bar{D}_r = \varepsilon_{33}\bar{E}_r + e_{31}\bar{\epsilon}_\theta + e_{33}\bar{\epsilon}_r. \end{aligned} \tag{6.8}$$

Electric boundary conditions and the first initial conditions are approximated exactly in the grid points. The initial conditions for velocities are approximated first with central differences, and then the fictitious time layer $t = -\tau$ is subsequently eliminated by using the first Eq. (6.1) for $r \in \omega_2$ and $t = 0$. In a similar manner, we approximate initial conditions involving time derivatives of φ_1 and φ_2. Finally, following a standard procedure (e.g. in [19], see Section 5), our "limiting" boundary conditions are approximated as follows:

$$\frac{v_0^{n+1} - 2v_0^n + v_0^{n-1}}{\tau^2} = \frac{2c_1^2}{h_1}\frac{v_1 - v_0}{h_1}, \qquad w_{N_3} = 0. \tag{6.9}$$

The interior and exterior of the cylinder are approximated in a straightforward manner. To get a second-order approximation for the first pair of matching boundary conditions, we apply the integro-interpolational approach (e.g. [2,19]) where we integrate Eq. (6.3) with respect to r in $[R_1 - h_1/2, R_1]$

$$\int_{R_1 - h_1/2}^{R_1} r\frac{\partial^2 \varphi_1}{\partial t^2}\,\mathrm{d}r = c_1^2 r\left.\frac{\partial^2 \varphi_1}{\partial r}\right|_{R_1} - c_1^2 r\left.\frac{\partial \varphi_1}{\partial r}\right|_{R_1 - h_1/2}, \tag{6.10}$$

and then approximate each term in (6.10) as follows:

$$\int_{R_1 - h_1/2}^{R_1} r\frac{\partial \varphi_1}{\partial t^2} \approx \frac{h_1}{2}\left(R_1 - \frac{h_1}{4}\right)\frac{v_{N_1}^{n+1} - 2v_{N_1}^n + v_{N_1}^{n-1}}{\tau^2},$$

$$c_1^2 r\left.\frac{\partial \varphi_1}{\partial r}\right|_{R_1} = c_1^2 r\left.\frac{\partial u}{\partial t}\right|_{R_1} \approx c_1^2 R_1 \frac{y_0^{n+1} - y_0^{n-1}}{2\tau}, \quad c_1^2 r\left.\frac{\partial \varphi_1}{\partial r}\right|_{R_1 - h_1/2} \approx c_1^2\left(R_1 - \frac{h_1}{2}\right)\frac{v_{N_1} - v_{N_1 - 1}}{h_1}.$$

This results in

$$\frac{h_1}{2}\left(R_1 - \frac{h_1}{4}\right)\frac{v_{N_1}^{n+1} - 2v_{N_1}^n + v_{N_1}^{n-1}}{\tau^2} = c_1^2\left(R_1\frac{y_0^{n+1} - y_0^{n-1}}{2\tau} - \left(R_1 - \frac{h_1}{2}\right)\frac{v_{N_1} - v_{N_1 - 1}}{h_1}\right). \tag{6.11}$$

For the exterior of the cylinder, we act similarly. As for the second pair of the matching boundary conditions, we integrate the first Eq. (6.1) with respect to r in $[R_1, R_1 + h_2/2]$

$$\int_{R_1}^{R_1 + h_2/2} \rho_2 r\frac{\partial^2 u}{\partial t^2} = (r\sigma_r)|_{R_1 + h_2/2} - (r\sigma_r)|_{R_1} - \int_{R_1}^{R_1 + h_2/2} \sigma_\theta\,\mathrm{d}r + F_1^1, \tag{6.12}$$

with $F_1^1 = \int_{R_1}^{R_1+h_2/2} rF\,\mathrm{d}r$, and then approximate each term in (6.12) as follows:

$$\int_{R_1}^{R_1+h_2/2} \rho_2 r \frac{\partial^2 u}{\partial t^2}\,\mathrm{d}r \approx \rho_2 \frac{h_2}{2}\left(R_1 + \frac{h_2}{4}\right)\frac{y_0^{n+1} - 2y_0^n + y_0^{n-1}}{\tau^2};$$

$$(r\sigma_r)|_{R_1} = -R_1 P_1 = R_1\rho_1\frac{\partial \varphi_1}{\partial t} \approx R_1\rho_1\frac{v_{N_1}^{n+1} - v_{N_1}^{n-1}}{2\tau}, \quad \int_{R_1}^{R_1+h_2/2} \sigma_\theta\,\mathrm{d}r \approx \frac{h_2}{2}(\bar{\sigma}_\theta)_1,$$

and finally note that $(r\sigma_r)|_{R_1+h_2/2} \approx (R_1 + h_2/2)(\bar{\sigma}_r)_1$ at "flux" points. This results in the following second-order approximation

$$\frac{\rho_2 h_2}{2}\left(R_1 + \frac{h_2}{4}\right)\frac{\Delta y_0^n}{\tau^2} = \left(R_1 + \frac{h_2}{2}\right)(\bar{\sigma}_r)_1 - R_1\frac{v_{N_1}^{n+1} - v_{N_1}^{n-1}}{2\tau} - \frac{h_2}{2}(\bar{\sigma}_\theta)_1 + F_1^1, \tag{6.13}$$

and a similar procedure is applied for the cylinder exterior. Note that the four approximations just derived ((6.11) and (6.13) and two others for the exterior region) represent a pair of systems of linear equations $A\boldsymbol{x} = \boldsymbol{b}$ with $\boldsymbol{x} \in \mathbb{R}^2$, $\boldsymbol{b} \in \mathbb{R}^2$. The first system of this pair should be solved with respect to $(v_{N_1}^{n+1}, y_0^{n+1})^{\mathrm{T}}$ for matrix $A = A_1$, and the second system should be solved with respect to $(y_{N_2}^{n+1}, w_0^{n+1})^{\mathrm{T}}$ for matrix $A = A_2$, where

$$A_1 = \begin{pmatrix} \dfrac{h_1}{2\tau^2}\left(R_1 - \dfrac{h_1}{4}\right) & -\dfrac{c_1^2 R_1}{2\tau} \\ \dfrac{R_1}{2\tau} & \rho_2\dfrac{h_2}{2\tau^2}\left(R_1 + \dfrac{h_2}{4}\right) \end{pmatrix},$$

$$A_2 = \begin{pmatrix} c_2^2\dfrac{R_2}{2\tau} & \dfrac{h_3}{2\tau^2}\left(R_2 + \dfrac{h_3}{4}\right) \\ \rho_2\dfrac{h_2}{2\tau^2}\left(R_2 - \dfrac{h_2}{4}\right) & \dfrac{R_2}{2\tau} \end{pmatrix}.$$

The resulting systems have positive determinates and their solution, supplemented by the procedure described in [12,13], allows us to find all unknown functions on the time-layer $n+1$, which in its turn allows us to compute the stresses and the acoustic pressure, and proceed to the next time level. The described algorithm has been applied to a series of numerical experiments aimed at the description of the dynamic behavior of hollow piezoceramic cylinders accounting for the acoustic coupling with the surrounding media. In Fig. 2, we present the time distribution of radial displacements on the external surface of the cylinder (left) for the case of time-varying potential of the electric field (right). In the presented situation $V = 0.5\cos(t)$ in the dimensionless variables (e.g. [16] and references therein). All computational experiments were performed for PZT-5A piezoceramic (see basic parameters e.g. in [9,16]). The coupling between the dynamic characteristics of the piezoceramic cylindrical shell and the surrounding acoustic media increases when the thickness of the shell decreases (presented results are for $R_1 = 0.95$ and $R_2 = 1$ considered in the dimensionless variables). The acoustic pressures of the surrounding media constrain the motion of the shell (and therefore the amplitudes of the radial displacements generally decreases), but this can be partly compensated by an appropriate choice of the

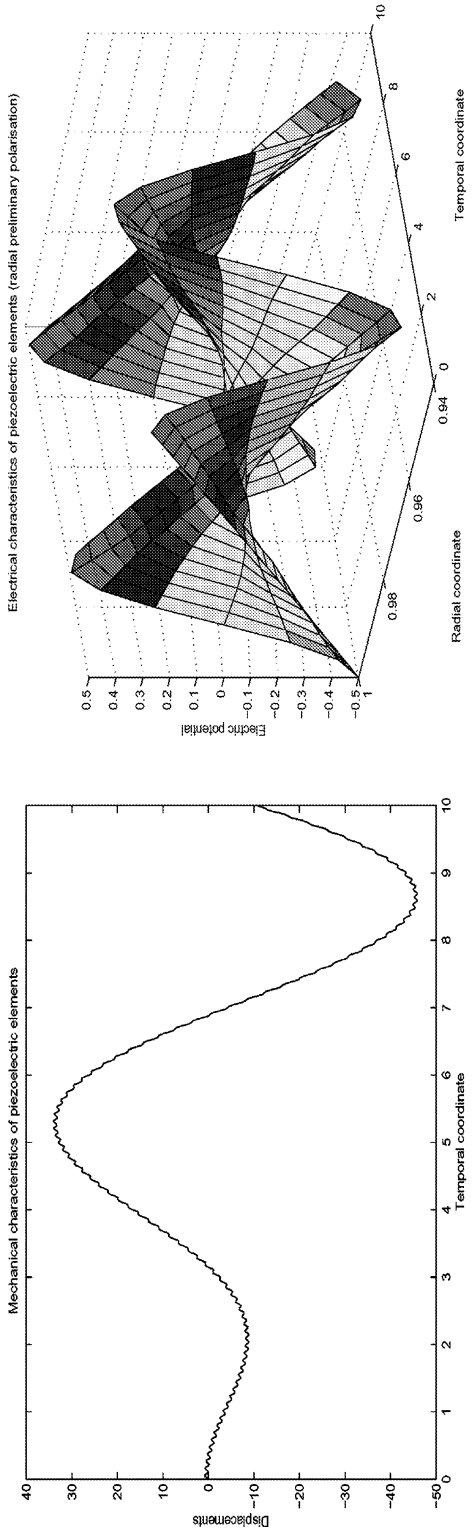

Fig. 2. The dynamics of radial displacements (left) and the electric potential (right) of the radially poled piezoceramic shell.

time-dependent electric loading since in the considered case the coupling between electric and mechanical field is strong.

Acknowledgements

The author thanks Dr. M. Willatzen for fruitful discussions on the topics related to this paper, and a referee for useful comments accounted for in the final version of the paper.

References

[1] M. Amabili, Free vibration of partially filled horizontal cylindrical shells, J. Sound Vibrat. 191 (1996) 757–780.
[2] M.M. Belova, M.N. Moskalkov, V.G. Savin, Numerical solution of the problem of sound emission by a cylindrical piezoelectric vibrator excited by electric pulses, J. Math. Sci. 63 (1993) 427–432.
[3] W.Q. Chen, Problems of radially polarised piezoelectric bodies, Int. J. Solids Struct. 36 (1999) 4317–4332.
[4] W.Q. Chen, Vibration theory of non-homogeneous, spherically isotropic piezoelastic bodies, Int. J. Sound Vibrat. 236 (2000) 833–860.
[5] P.C. Eccard, H. Landes, R. Lerch, Applications of finite element simulations to acoustic wave propagation within flowing media, Int. J. Comp. Appl. Technol. 11 (1998) 163–169.
[6] D.I. Fotiadis, G. Foutsitzi, C.V. Massalas, Wave propagation modeling in human long bones, Acta Mech. 137 (1999) 65–81.
[7] F. Gautier, N. Tahani, Vibroacoustics of cylindrical pipes: internal radiation modal coupling, J. Sound Vibrat. 215 (1998) 1165–1179.
[8] Y.M. Huang, C.R. Fuller, The effects of dynamic absorbers on the forced vibration of a cylindrical shell and its coupled interior sound field, J. Sound Vibrat. 200 (1997) 401–418.
[9] T. Ikeda, Fundamentals of Piezoelectricity, Oxford University Press, Oxford, 1990.
[10] F. Jacquemin, A. Vautrin, Contraintes transitoires thermoelastiques dans un cylindre creux stratifie anisotrope, C. R. Acad. Sci. Paris Mech. Solids Struct. Ser. 2 (1999) 963–969.
[11] L.E. Kinsler, Fundamentals of Acoustics, Wiley, NY, New York, 2000.
[12] R.V.N. Melnik, The stability condition and energy estimate for nonstationary problems of coupled electroelasticity, Math. Mech. Solids 2 (1997) 153–180.
[13] R.V.N. Melnik, Convergence of the operator-difference scheme to the generalized solutions of a coupled field theory, J. Differ. Equ. Appl. 4 (1998) 185–212.
[14] R.V.N. Melnik, K.N. Melnik, A note on the class of weakly coupled problems of non-stationary piezoelectricity, Commun. Numer. Method Eng. 14 (1998) 839–847.
[15] R.V.N. Melnik, Generilized solutions, discrete models and energy estimates for a 2D problem of coupled field theory, Appl. Math. Comp. 107 (2000) 27–55.
[16] R.V.N. Melnik, Computational analysis of coupled physical fields in piezothermoelastic media, Comp. Phys. Commun. 142 (1/3) (2001) 231–237.
[17] D. Royer, E. Dieulesaint, Elastic Waves in Solids, Springer, Berlin, 2000.
[18] M. Ruzzene, A. Baz, Active/passive control of sound radiation and power flow in fluid-loaded shells, Thin Walled Struct. 38 (2000) 17–42.
[19] A.A. Samarskii, The Theory of Difference Schemes, Marcel Dekker, NY, New York, 2001.
[20] N.A. Shulga, S.I. Melnik, Energy analysis of axisymmetric wave propagation in a hollow liquid-containing piezoelectric cylinder, Int. Appl. Mech. 32 (1996) 81–88.
[21] C.J. Wu, H.L. Chen, X.Q. Huang, Sound radiation from a finite fluid-filled/submerged cylindrical shell with porous material sandwich, J. Sound Vibrat. 238 (2000) 425–441.